Journal of Nuclear Materials 400 (2010) 8–14

Contents lists available at ScienceDirect

Journal of Nuclear Materials

journal homepage: www.elsevier.com/locate/jnucmat

# Diffuse reflectance and X-ray photoelectron spectroscopy of uranium in $ZrO_2$ and $Y_2Ti_2O_7$

E.R. Vance, Y. Zhang *, Z. Zhang

*Institute of Materials Engineering, Australian Nuclear Science and Technology Organisation, Locked Bag 2001, Kirrawee DC, NSW 2232, Australia*

ARTICLE INFO

*Article history:*
Received 15 October 2009
Accepted 3 February 2010

ABSTRACT

Diffuse reflectance measurements were made over the wavenumber range of 4000–20,000 $cm^{-1}$ at room temperature on monoclinic and stabilised $ZrO_2$, together with $Y_2Ti_2O_7$ having the pyrochlore structure, all of which were doped with U and sintered in various atmospheres. X-ray photoelectron spectroscopy measurements were also carried out on selected samples. In monoclinic and stabilised zirconia, U exhibited valence states of +4 and/or +5, depending on the sintering atmosphere and the presence of appropriate charge compensators. Using both diffuse reflectance and X-ray photoelectron spectroscopy, U was also observed as mainly $U^{4+}$ and/or $U^{5+}$ in U-doped $Y_2Ti_2O_7$ sintered at 1400 °C in air or Ar, although a small amount of $U^{6+}$ also appeared to be present in some U-doped $Y_2Ti_2O_7$ samples heated in air.



## 1. Introduction

In advanced fuel cycles, waste minor actinides from reprocessed nuclear fuels can be considered as potential fissile materials or burnable neutron absorbers yielding fertile components, or for immobilisation in glasses and ceramics. Candidate ceramics for immobilisation considered here are monoclinic and stabilised zirconia [1–3] and pyrochlore-structured titanates [4,5], and we are studying the possible formation of high actinide valence states in these materials with an ultimate aim of understanding how to suppress these higher valence states which can form actinyl ions and tend to enhance leaching. In these materials, the actinide would be expected on the basis of ionic size to substitute for Zr in zirconia or Y in $Y_2Ti_2O_7$. However this paper only deals with uranium.

Stabilised zirconia is also a strong candidate for use as an inert matrix fuel for actinide burning in reactors [2,6–9], and knowledge of actinide valences would aid in basic understanding of the material's behaviour during irradiation as fission products become available for reaction and/or substitution into the matrix, and in possible final geological disposal scenarios.

Studies of the valence of U dilutely incorporated in monoclinic or stabilised zirconia are sparse. Neutron irradiation of polycrystalline monoclinic zirconia containing ~0.4 wt.% of depleted U resulted in the formation of cubic zirconia arising from fission fragment damage [10]. Similar irradiation experiments on single crystals of monoclinic zirconia showed that the transformed cubic regions were partly coherent with the original structure and the U valence in the starting crystals was argued to be tetravalent [11]. However these flux-grown crystals exhibited their most intense electronic absorption peaks in the 6000–11,000 $cm^{-1}$ range so $U^{5+}$ was probably the dominant valence (see below). U was incorporated in urania–yttria electrode materials that were heated in contact with stabilised zirconia but no explicit U valence studies were made [12]. Also, X-ray absorption studies were made of (Er, Y, U, Zr)$O_{1.925}$ stabilised zirconia containing 0.1 formula units (f.u.) of U but the emphasis was on the local structure around the cations rather than the cation valences [13]. In a very recent study [14] yttria-stabilised zirconias containing U were sintered in argon at 1600 °C to encourage the U to be in the tetravalent form and this was confirmed in near-edge X-ray absorption work. Oxidation at 800 °C in air gave rise to an increase in U valence to a value between +5 and +6, as shown by the near-edge results. (Zr, Th, U) oxides were prepared by coprecipitation from aqueous solution; the precipitate was dried, calcined and finally sintered in an atmosphere of 3% $H_2$/1% $O_2$/96% Ar to attempt to reduce U to the tetravalent state [15]. However from X-ray absorption spectroscopy near the U $L_3$-edge, the U valence was determined to be >+4 (most likely because of the $O_2$ in the sintering atmosphere) and increase with increasing Zr content, but no features indicative of uranyl ions were observed.

Previous work [16] has been done on pyrochlore-structured $Nd_{1.8}U_{0.2}Zr_2O_{7+x}$ using X-ray absorption spectroscopy near the $L_3$-edge of U. In material sintered in Ar at 1650 °C, it was confirmed that U was in the tetravalent form. After further treatment at 800 °C in air, it was found that the average U valence was +5.5 and that no actinyl groups were present.

In the current work we have studied, by diffuse reflectance spectroscopy (DRS) over the ~4000–20,000 $cm^{-1}$ wavenumber range, together with X-ray photoelectron spectroscopy (XPS) of selected samples, different valence states of U in polycrystalline zirconia and pyrochlore-structured $Y_2Ti_2O_7$, noting that the principal

* Corresponding author. Tel.: +61 2 9717 9156; fax: +61 2 9543 7179.
*E-mail address:* yzx@ansto.gov.au (Y. Zhang).

0022-3115/$ - see front matter Crown Copyright © 2010 Published by Elsevier B.V. All rights reserved.
doi:10.1016/j.jnucmat.2010.02.003

constituents (Zr, Y, Ti and O) of these materials would not give rise to sharp electronic absorption bands in DRS in this range. While the actual energy levels responsible for the electronic absorption spectra of actinide ions are derived basically from the free ion states, they are also affected in detail by the magnitudes of spin–orbit and crystal-field interactions, so that the detailed spectrum of a given ion depends on its local environment in a solid or a liquid. Moreover the site symmetry is a key determinant of the sharpness and intensity of the absorption peaks. Electric dipole transitions give rise to much stronger transitions than magnetic dipole transitions, but sharp electric dipole absorptions (zero-phonon lines) are observed only when the ion lacks inversion symmetry. The very weak magnetic dipole transitions can give very weak zero-phonon lines when inversion symmetry is present, but most of the electronic absorption will derive from electric dipole transitions involving coupling with phonons (vibronic transitions) [17].

Since the U was targeted towards Zr in zirconia and Y sites in $Y_2Ti_2O_7$, the DRS absorption peaks were expected to be relatively sharp zero-phonon electric dipole transition bands because these sites in which the U was substituted lack inversion symmetry in all these materials. This can be seen from the appropriate space groups: $P2_1/c$ with Zr occupying the Wyckoff position 4*e* for monoclinic zirconia [18] and $P4_2/nmc$ with Zr at 2*b* for stabilised zirconia [19], as well as $Fd\text{-}3m$ with Y at 16*c* for pyrochlore-structured $Y_2Ti_2O_7$ [20]. The baseline valence states for U in refractory oxide-based ceramic hosts fired in air are $U^{4+}$, $U^{5+}$ and $U^{6+}$. Lowering the oxygen partial pressure or the use of a reducing atmosphere on sintering such oxides will tend to lower the actinide valence, but will not introduce $U^{3+}$ or lower U valence states.

Crystal-field stabilisation, including the presence of appropriate charge compensators, has the potential to lead to higher or lower U valence states. A well-known example of direct crystal-field stabilisation is found for Pu, where both $PuO_2$ ($Pu^{4+}$) and $PuPO_4$ ($Pu^{3+}$) are stable on firing in air at 1200 °C [21]. When Pu-doped $LaPO_4$ monazite ceramics are fired in air at 1000–1200 °C, the substitution of divalent Ca or Pb in the trivalent La site allows the valence of Pu to change from trivalent to tetravalent [22]. For U in brannerite ($UTi_2O_6$) in which U is normally tetravalent, the substitution of divalent or trivalent ions in the U site leads to the formation of $U^{5+}$ in both air and neutral (Ar) atmospheres [23–25]. Similar behaviour is found for U in zirconolite ($CaZrTi_2O_7$) [26], and zircon [27].

## 2. Experimental

Zirconia samples were made in both monoclinic and fully stabilised forms. In monoclinic zirconia, the U was simply substituted in the Zr sites to target the tetravalent U state $(Zr_{(1-z)}U_z)O_2$ or on the Zr sites with the U charge compensated by Y on the Zr sites $(Y_zZr_{(1-2z)}U_z)O_2$ to encourage the formation of $U^{5+}$ ($z = 0.01$). Throughout the text we will for convenience refer to such samples as having two formula units of O per molecule, even though the formal stoichiometries depend on the U valence. The corresponding stabilised zirconia samples had $Y_{0.14}Zr_{0.85}U_{0.01}O_{2-\delta}$ stoichiometries, where $\delta = 0.07$, 0.065 or 0.06 if the U has valences of +4, +5 or +6 respectively.

The stoichiometries of the pyrochlore-structured phases used were $[Ca_{(n+1)x}Y_{(2-(n+2)x)}U_x]Ti_2O_7$, where $n = 0$, 1 and 2 indicate U valences of +4, +5 and +6 respectively via charge balance.

To assist the reactivity of the ceramic samples to allow incorporation of the U in solid solution, the constituents were mixed in the liquid state before calcination and sintering. The zirconia samples were made by mixing zirconium tetra-tert-butoxide $[Zr(OC(CH_3)_3)_4]$ and aqueous Y/uranyl nitrate solutions in stoichiometric proportions, then stir-drying, calcining in air at ~750 °C, pelletising and finally sintering in various atmospheres (air, Ar or 3.5% $H_2/N_2$) at 1450 °C. The pyrochlore-based materials were made using stoichiometric mixtures of Ti alkoxide and aqueous Ca/Y/uranyl nitrate solutions, stir-drying, calcining in air at ~750 °C, and firing at 1400 °C. The samples in which U was targeted as $U^{4+}$ were fired in an argon atmosphere, while the others were fired in air. The use of reducing atmospheres was not contemplated for the pyrochlore-structured materials because of likely complications with $Ti^{4+}$ being reduced to $Ti^{3+}$, and the attendant formation of perovskite-structured $YTiO_3$.

Two Philips diffractometers were used for X-ray diffraction (XRD), employing Co or Cu Kα radiation. Scanning electron microscopy (SEM) on polished surfaces of samples was carried out on a JEOL 6400 machine run at 15 kV and fitted with a Tracor Northern TN5502 energy-dispersive spectrometer (EDS) which utilised a comprehensive range of standards for quantitative work [28]. Diffuse reflectance (DR) spectra were measured on coarsely polished (using SiC paper to give a 9.5 μm finish) pellets at ambient temperature using a Cary 500 spectrophotometer equipped with a Labsphere Biconical Accessory. Spectra are referenced to that of a Labsphere certified standard (Spectralon), and transformed into Kubelka–Munk (K–M) units, $F(R) = K/S = (1 - R)^2/2R$ [29], where $F(R)$ is the *remission* or K–M function, $R$ is the reflectance, $K$ and $S$ are absorption and scattering coefficients, respectively. Note the reflectance at any wavelength is a function of the $K/S$ ratio and the two absolute values cannot be obtained from the above equation. To measure a good quality DR spectrum, some factors in sample preparation need to be taken into account: (1) particle size: smaller sample particle size to reduce the surface reflection; (2) refractive index: sample dilution to reduce specular (mirror) reflectance component; (3) homogeneity: uniform sample for result reproducibility; and (4) sample thickness: at least 1.5 mm of sample for properly measuring light scattering. The actual depth analysed by DRS varies from 0.1 to 2.0 mm depending on the particle size, density and porosity of the material, and the absorption-dependent wavelength of the light radiation as well.

XPS measurements were performed in ultra-high vacuum with a VG ESCALAB 220i-XL system employing a monochromatic Al Kα (1486.6 eV) X-ray source. The X-ray gun was operated at 120 W, and the spectrometer pass energy was set at 20 eV for regional scans. The diameter of the analysis area was approximately 500 μm, much larger than the average grain size. Although the thickness of the probed surface layer was <10 nm, the surfaces used in the XPS study were freshly polished to a 0.5 μm diamond finish using chemically inert solvents (AR grade cyclohexane and acetone), and stored under vacuum overnight before being analysed. Based on previous studies of U-containing brannerite [24,25], samples prepared in this manner are representative of the bulk aside from a slight surface oxidation (<10%) due to exposure to air. The specimens were mounted under a stainless steel foil with an open aperture of approximately 3 mm in diameter. A low energy electron flood gun was used for the neutralisation of surface charge build-up in these insulating samples. The binding energies were calibrated by fixing the C 1 s peak (due to adventitious carbon) at 285.0 eV.

## 3. Results and discussion

### 3.1. Zirconia

The lattice parameters of the U-doped zirconia samples, as determined by XRD, were in good agreement with standard patterns (JCPDS 37–1484). There were no significant lattice parameter shifts, on doping with U and Y, because of the quite dilute nature of these substituents. The absence of any "extra" lines in the X-ray

patterns of the samples confirms that the U ions were fully incorporated in solid solution in these samples, noting the very high X-ray scattering power of U as compared to Zr.

Monoclinic samples of $Zr_{0.99}U_{0.01}O_2$ and $Y_{0.01}Zr_{0.98}U_{0.01}O_2$ nominal stoichiometries, together with the stabilised zirconia of $Y_{0.14}Zr_{0.85}U_{0.01}O_{(2-\delta)}$ stoichiometry were examined by DRS. The air-fired monoclinic samples (noting that the phase diagram [30] indicates more than about 6 mol.% of $YO_{1.5}$ is necessary to partly stabilise $ZrO_2$) gave a sharp absorption band which consisted of at least three closely spaced components at around 6580 $cm^{-1}$, together with weaker broad components centred at roughly 4000, 9400 and 13,000 $cm^{-1}$ (see Fig. 1b and c). The air-fired stabilised sample (Fig. 1a) gave a weak but quite sharp band at around 6360 $cm^{-1}$, together with a broad band centred at ~14,000 $cm^{-1}$.

Possible U valences would include +4 ($5f^2$ electronic configuration), +5 ($5f^1$) and +6 ($5f^0$) states (see Section 1). The $U^{4+}$ spectrum gives sharp (if a zero-phonon line) and broad (vibronic) absorptions right through the infrared and visible spectral range [27]. The $U^{5+}$ spectrum however is confined to the near infrared because it derives only from the crystal-field splittings of $^2F_{5/2} - {}^2F_{7/2}$ components (split by spin–orbit coupling) of the $U^{5+}$ $^2F$ electronic state, with majority electronic transitions observable from the splitting of $^2F_{7/2}$ at ~6900–14,000 $cm^{-1}$ [27]. However because $U^{6+}$ has no unpaired electrons, the only potentially observable electronic transitions are of a broad charge-transfer nature, occurring in the blue and near-ultraviolet spectral regions.

The sharp components of these spectra may therefore be attributed to relatively sharp zero-phonon electric dipole transitions of $U^{5+}$ [27]. The air-fired stabilised zirconia sample, $Y_{0.14}Zr_{0.85}U_{0.01}O_{(2-\delta)}$, could in principle contain $U^{6+}$ because of the relatively large $Y^{3+}$ component. Since DRS is not appropriate for $U^{6+}$ detection, this sample was also examined by XPS, which has the ability to distinguish between different U oxidation states based on the binding energy of U 4f levels. As the oxidation state of uranium increases from $U^{4+}$ ($UO_2$) to $U^{6+}$ ($UO_3$), the binding energy of the U $4f_{7/2}$ peak increases by 1.7–1.8 eV [31,32]. Although the stabilised zirconia sample was sintered in air, the U $4f_{7/2}$ XPS spectrum (see Fig. 2) suggests that only $U^{5+}$ and $U^{4+}$ (and not $U^{6+}$) are present in the sample. The presence of $U^{5+}$ is consistent with the DRS results as shown in Fig. 1a. However the absence of any DRS bands attributable to $U^{4+}$ is somewhat puzzling.

Polishing the sample of $Y_{0.14}Zr_{0.85}U_{0.01}O_{(2-\delta)}$ that was black in color after sintering in air exposed a yellow-colored interior when

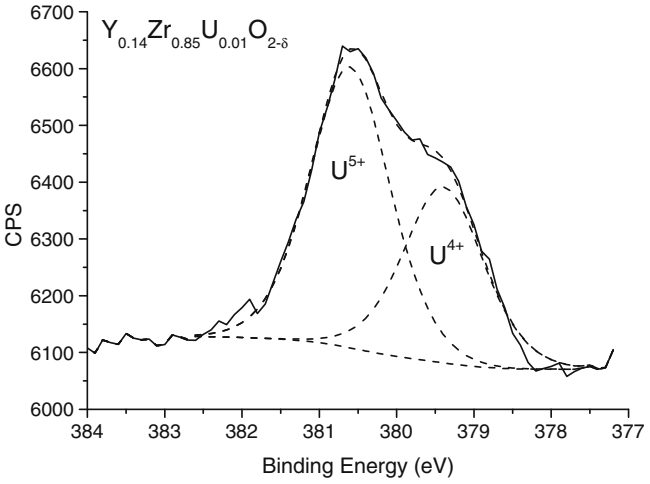


**Fig. 2.** U $4f_{7/2}$ XPS spectrum from stabilised zirconia $Y_{0.14}Zr_{0.85}U_{0.01}O_{(2-\delta)}$ (sintered in air), with peak fitting results indicating the presence of 62% of $U^{5+}$ and 38% of $U^{4+}$.

a few tenths of a mm of material was removed from the surface. However, DR spectra of the yellow-colored material were similar to those obtained from the black-colored original surface, although there was decreased absorption in the visible and near infrared regions of the spectrum. Moreover heating the sample in the $H_2/N_2$ atmosphere to a temperature of 1450 °C yielded no bands attributable to $U^{4+}$ (see Fig. 3c). While on the subject of U DRS in stabilised zirconia, optical absorption data on a transparent single crystal of stabilised zirconia were previously attributed to $U^{4+}$ [33]. But SEM examination of this crystal in the present work showed that an appreciable amount of Nd was present (the respective Zr, Hf, Y, Nd and U contents from SEM analysis were 0.82, 0.02, 0.14, 0.01 and 0.002 f.u. respectively). Of these elements, Zr and Hf would occur as tetravalent ions and Y would be trivalent and so they would have no unfilled electron shells and would therefore not give any DRS peaks. Only $U^{4+}$, $U^{5+}$ and $Nd^{3+}$ would have unfilled shells and give rise to DRS peaks.

DRS data on polycrystalline Nd-doped stabilised zirconia of nominal composition $Nd_{0.01}Y_{0.14}Zr_{0.85}O_{1.925}$ sintered for 12 h at 1500 °C in air showed that all the absorption peaks previously

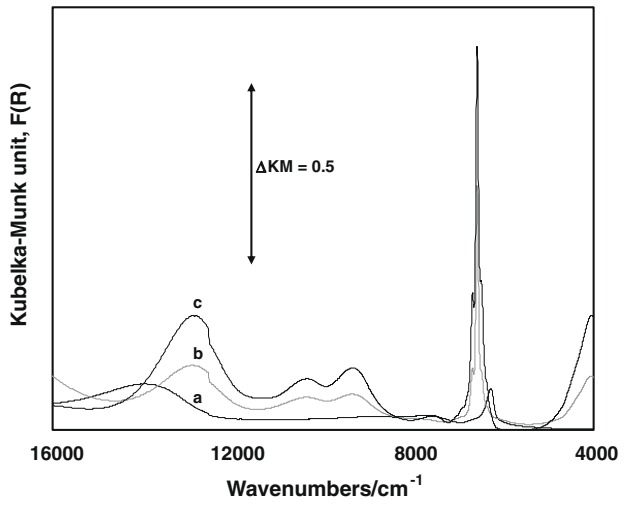


**Fig. 1.** DR spectra (4000–16,000 $cm^{-1}$) of: (a) $Y_{0.14}Zr_{0.85}U_{0.01}O_{(2-\delta)}$; (b) $Y_{0.01}Zr_{0.98}U_{0.01}O_2$; and (c) $Zr_{0.99}U_{0.01}O_2$ samples sintered in air at 1450 °C (ΔKM is used as the spectra are offset vertically to enhance visibility).

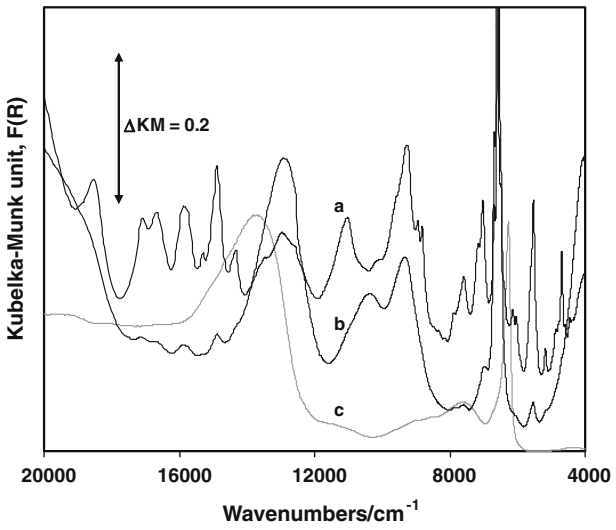


**Fig. 3.** DR spectra (4000–20,000 $cm^{-1}$) of: (a) $Zr_{0.99}U_{0.01}O_2$; (b) $Y_{0.01}Zr_{0.98}U_{0.01}O_2$; and (c) $Y_{0.14}Zr_{0.85}U_{0.01}O_{(2-\delta)}$ samples (all formulae nominal) sintered in 3.5% $H_2/N_2$ at 1450 °C (ΔKM is used as the spectra are offset vertically to enhance visibility).

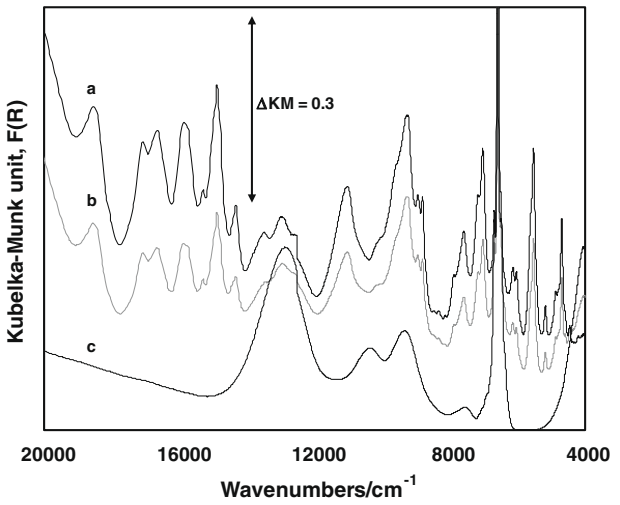


**Fig. 4.** DR spectra (4000–20,000 $cm^{-1}$) of uncompensated monoclinic $Zr_{0.99}U_{0.01}O_2$ samples (formulae nominal) reheated at 1450 °C in: (a) 3.5% $H_2/N_2$, (b) argon, and (c) as-sintered in air at 1450 °C (ΔKM is used as the spectra are offset vertically to enhance visibility).

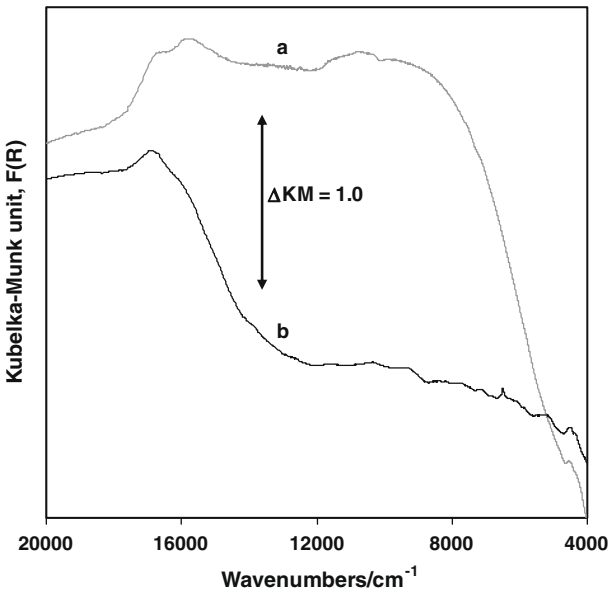


**Fig. 5.** DR spectra (4000–20,000 $cm^{-1}$) of: (a) $Ca_{0.1}Y_{1.8}U_{0.1}Ti_2O_7$; and (b) $Ca_{0.3}Y_{1.4}U_{0.3}Ti_2O_7$ (all formulae nominal) sintered at 1400 °C in Ar targeting $U^{4+}$ (ΔKM is used as the spectra are offset vertically to enhance visibility).

**Table 1**
U valence states in zirconia samples from DRS.

| Sample | Sintering atmosphere | Measured U valence |
|---|---|---|
| Uncompensated $(Zr_{0.99}U_{0.01})O_2$ | Air | $U^{5+}$ |
| | Ar | $U^{4+} + U^{5+}$ |
| | $N_2/H_2$ | $U^{4+} + U^{5+}$ |
| Compensated | Air | $U^{5+}$ |
| $(Y_{0.01}Zr_{0.98}U_{0.01})O_2$ | $N_2/H_2$ | $U^{5+}$ + tr. $U^{4+}$ |
| Stabilised $(Y_{0.14}Zr_{0.85}U_{0.01})O_{2-\delta}$ | Air | $U^{5+}$ $ |
| | $N_2/H_2$ | $U^{5+}$ |

$ XPS showed ~62% $U^{5+}$ +38% $U^{4+}$.

attributed to $U^{4+}$ in the single crystal were actually due to $Nd^{3+}$, with the exception of a peak at ~6700 $cm^{-1}$ which, from the present data on U in stabilised zirconia, we now attribute to $U^{5+}$.

Heating the uncompensated monoclinic $Zr_{0.99}U_{0.01}O_2$ sample in argon or $H_2/N_2$ at 1450 °C allowed the formation of many new absorption bands right across the range of 4000–20,000 $cm^{-1}$ and marked diminution of the bands attributed above to $U^{5+}$ (see Figs. 3a and 4). The new bands are consistent with broad expectations for the $U^{4+}$ spectrum insofar as they were observed right across the visible and near infrared parts of the spectrum [26]. However the compensated monoclinic sample gave rise to only very weak $U^{4+}$ bands in addition to $U^{5+}$ bands on subsequent $H_2/N_2$ heat-treatment (see Fig. 3b), and the spectrum of the stabilised material remained essentially unchanged (Fig. 3c). Here it is supposed that the effect of the $Y^{3+}$ dopants outweighed the effect of the reducing atmosphere. The failure to observe DRS absorption bands in this latter sample before and after reduction is not understood, unless the $U^{4+}$ ions observed by XPS in the oxidised sample

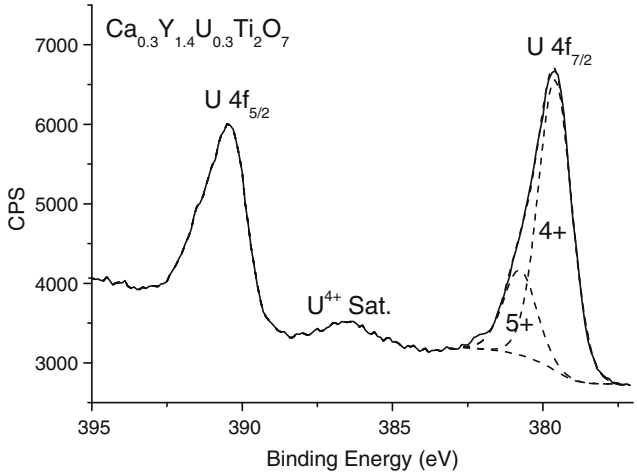


**Fig. 6.** U $4f_{7/2}$ XPS spectrum from $Ca_{0.3}Y_{1.4}U_{0.3}Ti_2O_7$ (sintered in Ar). Deconvolution of the U $4f_{7/2}$ peak indicates 77% of $U^{4+}$ and 23% of $U^{5+}$.

**Table 2**
U valence states and lattice parameters in $Y_2Ti_2O_7$ samples.

| Sample | Sintering atmosphere | Targeted U valence | Measured U valence | Lattice parameter (nm) |
|---|---|---|---|---|
| $Ca_{0.1}Y_{1.8}U_{0.1}Ti_2O_7$ | Ar | +4 | – (DRS) 90% $U^{4+}$, 10% $U^{5+}$ (XPS) | $1.011_2$ |
| $Ca_{0.3}Y_{1.4}U_{0.3}Ti_2O_7$ (*) | Ar | +4 | tr. $U^{5+}$ (DRS) 77% $U^{4+}$, 23% $U^{5+}$ (XPS) | $1.011_2$ |
| $Ca_{0.2}Y_{1.7}U_{0.1}Ti_2O_7$ | air | +5 | $U^{5+}$ (DRS) 71% $U^{5+}$, 19% $U^{4+}$ and 10% $U^{6+}$ (XPS) | $1.011_5$ |
| $Ca_{0.6}Y_{1.1}U_{0.3}Ti_2O_7$ | air | +5 | $U^{5+}$ (DRS) 83% $U^{5+}$, 17% $U^{6+}$ (XPS) | $1.012_1$ |
| $Ca_{0.15}Y_{1.8}U_{0.05}Ti_2O_7$ | air | +6 | – (DRS) | $1.009_9$ |
| $Ca_{0.9}Y_{0.8}U_{0.3}Ti_2O_7$ ($) | air | +6 | – (DRS) 83% $U^{5+}$, 17% $U^{6+}$ (XPS) | $1.013_2$ |

*Note*: * and $ denote weak lines due to the presence of $UO_2$ and perovskite, respectively.
– Represents no significant sharp absorption band signatures of any U valence states in DRS spectra. XPS observations of $U^{6+}$ can be partly attributed to surface oxidation (see text).

occupy centrosymmetric sites. DRS results on all zirconia samples are summarised in Table 1.

### 3.2. $Y_2Ti_2O_7$-based samples

XRD and SEM showed that the U-doped $Y_2Ti_2O_7$ samples in which U was targeted as $U^{4+}$ or $U^{5+}$ were very close to single-phase pyrochlore structures (see JCPDS card 42–413; lattice parameter 1.0095 nm) although the $Ca_{0.3}Y_{1.4}U_{0.3}Ti_2O_7$ sample showed very weak XRD peaks from $UO_2$-rich inclusions, attributed to a very slight chemical imbalance between the Ca and the U additions. The pyrochlore phase showed a slight lattice expansion due to Ca/U-doping (see Table 2). The expansion is attributed to (a) the larger ionic size [34] of $Ca^{2+}$ (0.112 nm in the 8-fold coordination of the Y site) as compared to $Y^{3+}$ (0.1019 nm) outweighing the slightly smaller ionic size of $U^{4+}$ (0.100 nm) compared to that of $Y^{3+}$ for the samples in which U was targeted as $U^{4+}$. The larger ionic size of $Ca^{2+}$ compared to that of $Y^{3+}$ was essentially cancelled out by the 8-fold ionic size of $U^{5+}$ (~0.09 nm, extrapolated from data for 6- and 7-fold coordination [34]) being smaller than $Y^{3+}$ in the samples in which $U^{5+}$ was targeted, but these samples contained twice as much $Ca^{2+}$ as $U^{5+}$, so again a lattice expansion would be predicted.

Samples in which $x = 0.1$ f.u. of U was targeted as $U^{4+}$ ($Ca_{0.1}Y_{1.8}U_{0.1}Ti_2O_7$, sintered in Ar) showed very broad peaks in the 4000–18,000 $cm^{-1}$ range on top of broad band absorption, while the sample containing 0.3 f.u. of U ($Ca_{0.3}Y_{1.4}U_{0.3}Ti_2O_7$) showed a broad absorption peak only over the 14,000–18,000 $cm^{-1}$ range on top of broad band absorption (and the intensity of which is lower than the corresponding broad band absorption of the $x = 0.1$ sample) (Fig. 5). The origins of this broad absorption are not clear at this point but are most likely due to intervalence charge-transfer between $U^{4+}$, $U^{5+}$ and $Ti^{4+}$ and possibly very small amounts of $Ti^{3+}$. The very weak sharp absorption band at ~6700 $cm^{-1}$ in the $Ca_{0.3}Y_{1.4}U_{0.3}Ti_2O_7$ sample (U targeted as $U^{4+}$) is assigned to small amounts of $U^{5+}$, which was confirmed by XPS (Fig. 6). In addition to the binding energy of the U $4f_{7/2}$ XPS peak, the satellite peak (marked as "Sat.") associated with the U 4f level is also very sensitive to the U oxidation state

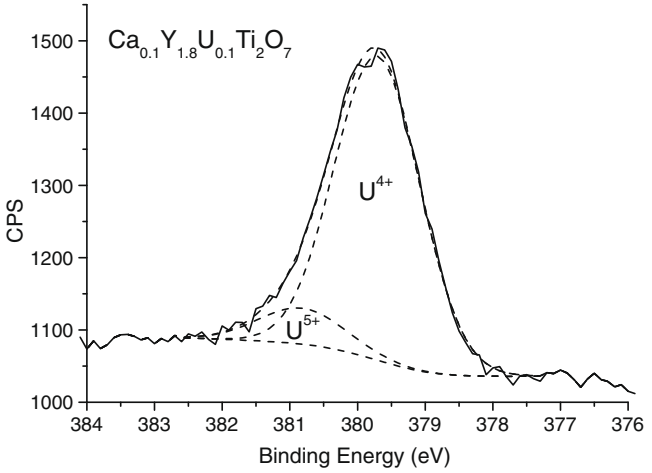


**Fig. 7.** U $4f_{7/2}$ XPS spectrum from $Ca_{0.1}Y_{1.8}U_{0.1}Ti_2O_7$ (sintered in Ar). Deconvolution of the U $4f_{7/2}$ peak indicates 90% of $U^{4+}$ and 10% of $U^{5+}$.

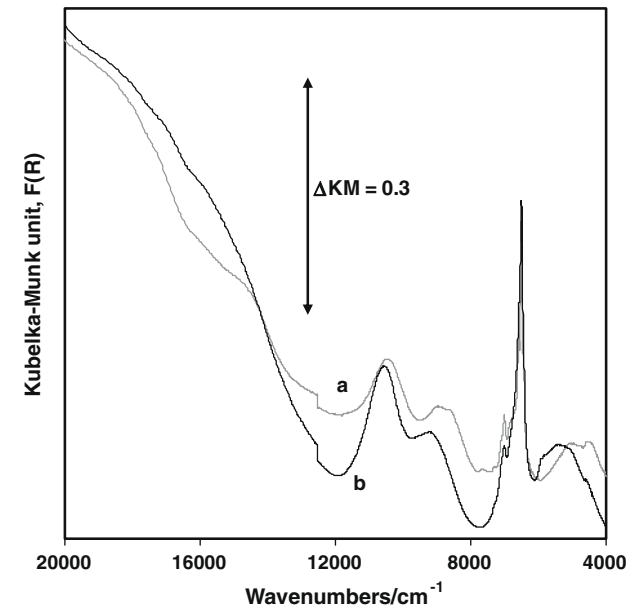


**Fig. 8.** DR spectra (4000–20,000 $cm^{-1}$) of: (a) $Ca_{0.2}Y_{1.7}U_{0.1}Ti_2O_7$, and (b) $Ca_{0.6}Y_{1.1}U_{0.3}Ti_2O_7$ sintered at 1400 °C in air, targeting $U^{5+}$ (ΔKM is used as the spectra are offset vertically to enhance visibility).

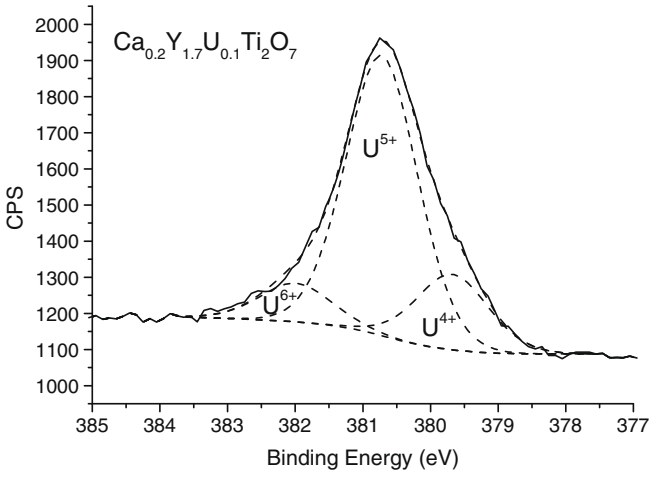


**Fig. 9.** U $4f_{7/2}$ XPS spectrum from $Ca_{0.2}Y_{1.7}U_{0.1}Ti_2O_7$ (sintered in air). Deconvolution of the U $4f_{7/2}$ peak indicates 71% of $U^{5+}$, 19% of $U^{4+}$ and 10% of $U^{6+}$.

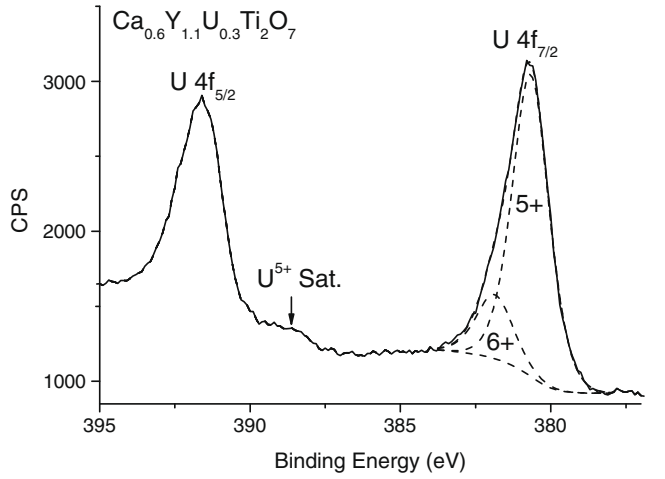


**Fig. 10.** U 4f XPS spectrum from $Ca_{0.6}Y_{1.1}U_{0.3}Ti_2O_7$ (sintered in air). Deconvolution of the U $4f_{7/2}$ peak indicates 83% of $U^{5+}$ and 17% of $U^{6+}$.

[24,25,35]. Note the amount of $U^{4+}$ detected by XPS includes the contribution from the $UO_2$ impurity phase in this sample. XPS measurements of the $Ca_{0.1}Y_{1.8}U_{0.1}Ti_2O_7$ sample (Fig. 7) also confirmed that the U valence was predominantly 4+, and the small amount of $U^{5+}$ (~10%) is largely attributed to surface oxidation. Note that the U satellite peak associated with $U^{4+}$ in this sample was too weak to be observed (due to the low U content).

The absence of discernible $U^{4+}$ peaks in the DRS data is possibly attributed to intervalence charge-transfer absorption between U and possibly Ti ions of different valence, which is very likely to yield the observed broad band absorption in these samples and of course would serve to obliterate weak sharp zero-phonon bands.

Samples in which 0.1 and 0.3 f.u. of U ($Ca_{0.2}Y_{1.7}U_{0.1}Ti_2O_7$ and $Ca_{0.6}Y_{1.1}U_{0.3}Ti_2O_7$) was targeted as $U^{5+}$ showed broad, probably phonon-assisted bands in the vicinity of 5000–6000 $cm^{-1}$ and 7000–12,000 $cm^{-1}$, with these wavenumber ranges as expected for $U^{5+}$ [23,26]. In addition there were sharp zero-phonon lines at ~6700 $cm^{-1}$ (see Fig. 8), characteristic of $U^{5+}$. The U XPS spectra obtained from these two samples (Figs. 9 and 10) confirmed that the U oxidation state was predominantly 5+ in both samples. The $Ca_{0.2}Y_{1.7}U_{0.1}Ti_2O_7$ sample (Fig. 9) also contained a small amount of $U^{4+}$ (~19%), while the $U^{6+}$ (~10%) component in this sample is attributed to surface oxidation. The $U^{6+}$ (~17%) component in the $Ca_{0.6}Y_{1.1}U_{0.3}Ti_2O_7$ sample (Fig. 10), however, is larger than what would be expected from surface oxidation alone based on previous XPS studies of U-containing titanates [24,25].

The sample in which 0.3 f.u. of U ($Ca_{0.9}Y_{0.8}U_{0.3}Ti_2O_7$) was targeted as $U^{6+}$ showed 5–10 volume percent of essentially U-free perovskite of composition $Ca_{0.81}Y_{0.11}Ti_{1.01}O_3$ (see SEM image in Fig. 11), that approximates to $Ca_{(1-3x/2)}Y_xTiO_3$ in which cation vacancies are the charge compensators for Y substituted on Ca sites. The composition of the pyrochlore, $Ca_{0.74}Y_{0.90}U_{0.34}Ti_{2.02}O_7$, was consistent with expectations based on the idea that the U was actually all present as $U^{5+}$. XRD showed weak perovskite peaks in addition to those from the majority pyrochlore phase (see Fig. 12). The DR spectrum (not shown here) showed only broad absorption, roughly similar to the results shown in Fig. 5a and no

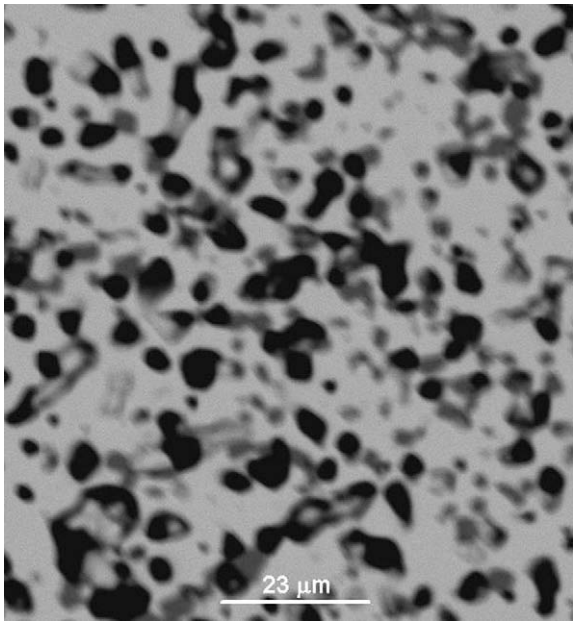


**Fig. 11.** Backscattered electron micrograph of sample composition $Ca_{0.9}Y_{0.8}U_{0.3}Ti_2O_7$ targeting U as $U^{6+}$; light areas = pyrochlore matrix, grey areas = perovskite; dark areas = pores.

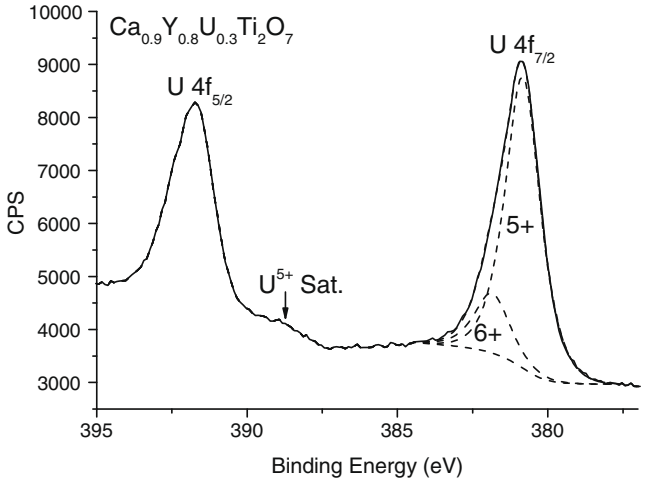


**Fig. 13.** U 4f XPS spectrum from $Ca_{0.9}Y_{0.8}U_{0.3}Ti_2O_7$ (sintered in air). Deconvolution of the U $4f_{7/2}$ peak indicates 83% of $U^{5+}$ and 17% of $U^{6+}$.

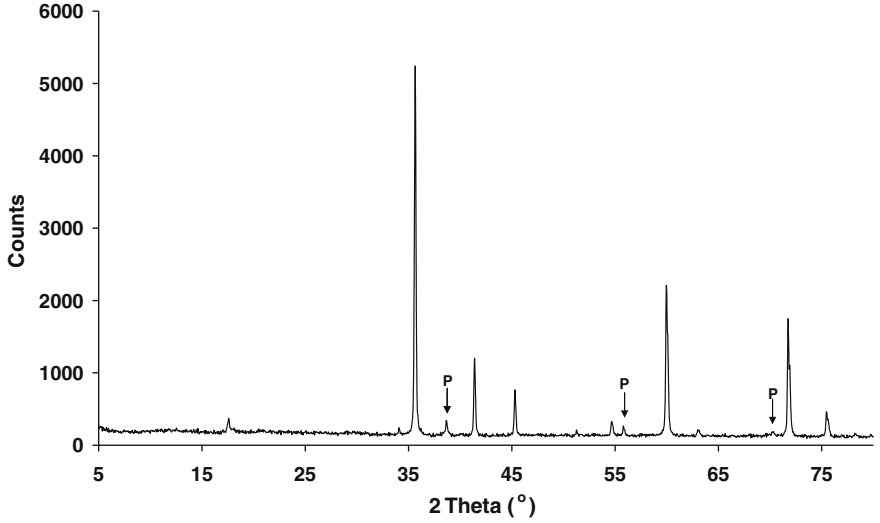


**Fig. 12.** XRD of $U^{6+}$-targeted sample ($Ca_{0.9}Y_{0.8}U_{0.3}Ti_2O_7$) fired in air; *P* = perovskite, Co Kα radiation.

indication of $U^{5+}$ peaks. Again the broad band absorption is attributed to strong intervalence charge-transfer absorption between $U^{5+}$ and $U^{6+}$. To follow up this notion, XPS measurements were undertaken and the results confirmed that the uranium oxidation state is predominantly +5 in this sample (Fig. 13), but with a small amount of $U^{6+}$ detected (~17%). Again, although this could derive from a thin oxidised surface layer, our previous XPS studies suggest the amount of surface oxidation is usually <10% in U-containing titanates [24,25].

Assuming all the U remains as $U^{5+}$ and it all enters the pyrochlore, the solid state chemistry is shown in the equation (correct to two significant figures only): $Ca_{0.9}Y_{0.8}U_{0.3}Ti_2O_7 \rightarrow 0.83\ [Ca_{0.72}Y_{0.92}U_{0.36}Ti_2O_7] + 0.17\ [Ca_{0.87}Y_{0.14}Ti_{0.98}O_3] + 0.075\ O_2$, and this phase assemblage gave reasonable agreement with the SEM results. However this does not negate the XPS evidence of a small amount of $U^{6+}$ being present.

## 4. Conclusions

In monoclinic and stabilised zirconia, U exhibited valence states of +4 and/or +5, in DRS and XPS spectra, depending on the sintering atmosphere and the presence of appropriate charge compensators. However no sign of single-ion $U^{4+}$ was observed in oxidised or reduced stabilised zirconia using DRS even though the presence of significant $U^{4+}$ was determined using XPS measurements in the oxidised sample, and this behaviour remains to be understood.

Only $U^{5+}$ was definitely observed by DRS in U-doped $Y_2Ti_2O_7$ pyrochlores sintered at 1400 °C in air or Ar, but $U^{4+}$ was clearly observable by XPS in the samples sintered in Ar. Observation of single-ion U spectra in the pyrochlore samples was complicated by the presence of strong broad band absorption attributable to intervalence charge transfer phenomena. Even though the SEM and XRD data were consistent with the U being in the form of $U^{5+}$, XPS results obtained from the sample with U targeted as $U^{6+}$ ($Ca_{0.9}Y_{0.8}U_{0.3}Ti_2O_7$ sintered in air) indicated that while $U^{5+}$ was the predominant component in the sample, a small percentage of $U^{6+}$ was present. Further clarification of these ideas could be made using X-ray near-edge absorption spectroscopy and such measurements are planned in future work.

To minimise leaching effects from ground water, avoidance of higher valence states of actinides substituted in zirconia and $Y_2Ti_2O_7$ waste forms should be assured by attention to the presence of charge compensators and the use of low-oxygen processing atmospheres. However this needs verification for Np and Pu and this also will be the subject of future work.

## Acknowledgments

We thank T. McLeod, A. Gillen, G. Smith, C. Jennison and T. Palmer for assistance with sample preparation, A. Day for scanning electron microscopy and T. McLeod and A. Gillen for X-ray diffraction. We are also grateful to Dr. B. Gong of University of New South Wales for his help with the XPS measurements. Finally, we thank anonymous reviewers for constructive comments on earlier drafts of the manuscript.

## References

[1] H. Kinoshita, K. Kuramoto, M. Uno, S. Yamanaka, H. Mitamura, T. Banba, Chemical durability of yttria-stabilized zirconia for highly concentrated TRU wastes, in: R.W. Smith, D.W. Shoesmith (Eds.), Scientific Basis for Nuclear Waste Management XXIII, Materials Research Society, Warrendale, PA, USA, 2000, pp. 393–398.
[2] W.L. Gong, W. Lutze, R.C. Ewing, J. Nucl. Mater. 277 (2000) 239–249.
[3] R.B. Heimann, T.T. Vandergraaf, J. Mater. Sci. Lett. 7 (1988) 583–586.
[4] E.R. Vance, A. Jostsons, S. Moricca, M.W.A. Stewart, R.A. Day, B.D. Begg, M.J. Hambley, K.P. Hart, B.B. Ebbinghaus, Synroc derivatives for excess weapons plutonium, in: J.C. Marra, G.T. Chandler (Eds.), Ceramics Transactions (Environmental Issues and Waste Management Technologies IV), vol. 93, American Ceramic Society, 1999, pp. 323–329.
[5] S.G. Cochran, W.H. Dunlop, T.A. Edmunds, L.M. MacLean, T.H. Gould, Fissile Material Disposition Program-Final Immobilization Form Assessment and Recommendation, UCRL-ID-128705 (1997).
[6] H. Kleykamp, J. Nucl. Mater. 275 (1999) 1–11.
[7] C. Degueldre, J.M. Paratte, J. Nucl. Mater. 274 (1999) 1–6.
[8] C. Degueldre, J. Alloys Compd. 444–445 (2007) 36–41.
[9] M.W.A. Stewart, E.R. Vance, J. Aust. Ceram. Soc. 42 (2006) 50–66.
[10] M.C. Wittels, J.O. Steigler, F.A. Sherrill, J. Nucl. Energy Parts A/B 16 (1962) 237–244 (Reactor Science and Technology).
[11] E.R. Vance, J.N. Boland, Rad. Eff. 37 (1978) 237–239.
[12] S.P.S. Badwal, F.T. Ciacchi, D.K. Sood, Solid State Ionics 18–19 (1986) 1033–1037.
[13] S.D. Conradson, C.A. Delguedre, F.J. Espinosa-Faller, S.R. Foltyn, K.E. Sickafus, J.A. Valdez, P.M. Villella, Prog. Nucl. Energy 38 (2001) 221–230.
[14] M. Walter, J. Somers, D. Bouexiere, P. Gaczynski, B. Brendebach, J. Solid State Chem. 182 (2009) 3305–3311.
[15] G. Curran, Y. Sevestre, W. Rattray, P. Allen, K.R. Czerwinski, J. Nucl. Mater. 323 (2003) 41–48.
[16] C. Nastren, R. Jardin, J. Somers, M. Walter, B. Bredenbach, J. Solid State Chem. 182 (2009) 1–7.
[17] F.A. Cotton, G. Wilkinson, Advanced Inorganic Chemistry: A Comprehensive Text, fifth ed., John Wiley and Sons, 1988.
[18] D.K. Smith, H.W. Newkirk, Acta Cryst. 18 (1965) 983–991.
[19] M. Yashima, S. Sasaki, M. Kakihana, Y. Yamaguchi, H. Arashi, M. Yoshimura, Acta Cryst. B 50 (1994) 663–672.
[20] M. Glerup, O.F. Nielsen, F.W. Poulsen, J. Solid State Chem. 160 (2001) 25–32.
[21] C.J. Bjorklund, J. Amer. Chem. Soc. 79 (1958) 6347–6350.
[22] Y. Zhang, E.R. Vance, J. Nucl. Mater. 374 (2008) 192–196.
[23] E.R. Vance, J.N. Watson, M.L. Carter, R.A. Day, B.D. Begg, J. Amer. Ceram. Soc. 84 (2001) 141–144.
[24] K.S. Finnie, Z. Zhang, E.R. Vance, M.L. Carter, J. Nucl. Mater. 317 (2003) 46–53.
[25] M. Colella, G.R. Lumpkin, Z. Zhang, E.C. Buck, K.L. Smith, Phys. Chem. Minerals 32 (2005) 52–64.
[26] E.R. Vance, G.R. Lumpkin, D.J. Cassidy, C.J. Ball, R.A. Day, B.D. Begg, J. Amer. Ceram. Soc. 85 (2002) 1853–1859.
[27] E.R. Vance, D.J. Mackey, Phys. Rev. B18 (1978) 185–190.
[28] G.R. Lumpkin, K.L. Smith, M.G. Blackford, R. Giere, C.T. Williams, Micron 25 (1994) 581–588.
[29] W.W. Wendlandt, H.G. Hecht, Reflectance Spectroscopy, Wiley Interscience, New York, 1966.
[30] H.G. Scott, J. Mater. Sci. 10 (1975) 1527–1535.
[31] D. Chadwick, Chem. Phys. Lett. 21 (1973) 291–294.
[32] G.C. Allen, J.A. Crofts, M.T. Curtis, P.M. Tucker, D. Chadwick, P.J. Hampson, J. Chem. Soc. Dalton Trans. (1974) 1296–1301.
[33] E.R. Vance, Mater. Res. Bull. 21 (1986) 321–329.
[34] R.D. Shannon, Acta Cryst. A 32 (1976) 51–67.
[35] J.-H. Liu, S. Van den Berghe, M.J. Konstantinovic, J. Solid State Chem. 182 (2009) 1105–1108.